POLITECNICO DI TORINO
Repository ISTITUZIONALE

Phase field approach for managing multi-fragment interactions in load-bearing fractured media

Original
Phase field approach for managing multi-fragment interactions in load-bearing fractured media / Chao Correas, A., Acquesta, D., Corrado, M.. - In: INTERNATIONAL JOURNAL OF FRACTURE. - ISSN 0376-9429. - 250:1(2025), pp. 1-17. [10.1007/s10704-025-00843-5]

Availability:
This version is available at: 11583/2999147 since: 2025-04-14T10:44:53Z

Publisher:
Springer

Published
DOI:10.1007/s10704-025-00843-5

Terms of use:

This article is made available under terms and conditions as specified in the corresponding bibliographic description in the repository

Publisher copyright

(Article begins on next page)

18 November 2026

Int J Fract
https://doi.org/10.1007/s10704-025-00843-5

RESEARCH

Phase field approach for managing multi-fragment interactions in load-bearing fractured media

A. Chao Correas · D. Acquesta · M. Corrado

Received: 8 August 2024 / Accepted: 8 February 2025
© The Author(s) 2025

Abstract This work introduces a novel approach for characterizing the residual load bearing capacity of fractured components based on the Phase Field fracture model. The underlying idea involves exploiting this well-established framework for fracturing materials and applying it to mechanically loaded domains in which fracture has already occurred. Hence, the continuous phase field here portrays the smeared representation of known crack patterns, based on which the unilateral contact interactions between the crack lips are enforced through a suitable strain energy decomposition. This allows for a theoretically robust and implicit treatment of the originally discontinuous problem while remaining in a continuum framework. As such, the proposed approach avoids the numerically challenging definition and management of conventional contact pairs, thus proving to be especially promising for its application to domains with multiple fragments. Besides presenting the theoretical foundation and algorithmic convenience of the approach, its accuracy and representativeness are proven against theoretical predictions and numerical results from Finite Element models featuring conventional contact interactions.

A. Chao Correas · D. Acquesta · M. Corrado (✉)
Department of Structural, Geotechnical and Building Engineering, Politecnico di Torino, Turin, Italy
e-mail: mauro.corrado@polito.it

Keywords Phase field fracture model · Fractured materials · Load bearing capacity · Unilateral contact interactions

1 Introduction

The presence of cracks causes the localized loss of structural continuity in mechanical components and heavily compromises their load-bearing capacity. However, the effective increase in compliance showcased by fractured structures is not total, since it mainly manifests under tensile and shear dominated stress conditions. In contrast, cracks can still transmit compressive stresses across, often to the same extent as in pristine conditions. This occurs because of the unilateral contact interactions arising so as to avoid interpenetration between fragments, which in turn result in a non-negligible load-bearing capacity even for largely fractured media. As such, the development of robust methodologies able to reproduce the interactions between the existent fragments is of great interest for both capturing the post-fracture mechanical performance and ascertaining the safety of critical structural systems. Among others, one can mention the case of multi-layered materials, such as laminated glass, whose post-fracture load bearing capacity is provided by the interaction among fractured and intact plies (Biolzi et al. 2018; Nielsen et al. 2022); and the case of micro-structured materials, in which the fragments' topol-

Published online: 24 February 2025

ogy and layer arrangement are engineered to improve mechanical properties (Yin et al. 2019).

The biggest difficulty in predicting the residual performance of fractured structures resides in properly reproducing the complex interactions between the different fragments, especially when they are numerous and complex in shape. This renders necessary the use of computational approaches to determine the mechanical state of the fractured domain upon loading, among which the Finite Element method is a prominent choice. However, conventional Finite Element formulations are not able to deal with unilateral contact interactions between fragments, hence requiring an enrichment of the formulation. In that regard, the most straightforward approach consists in modelling a discrete representation of the fragments, i.e. one in which each of them is treated as an individual deformable domain subjected to some contact pressure along its boundary so as to avoid penetrating the neighboring fragments. These interactions can be then enforced in many ways, *inter alia* cohesive interfaces or penalty-based contact surfaces, although at the cost of considerably high computational cost as well as increased pre-processing and resolution complexity; so much so that, to the best of the Authors' knowledge, there are only very recent and simplified studies specifically devoted to the structural assessment of fractured domains using this approach (see e.g. Bedon and Fasan 2024). Conversely, such discrete models have been extensively exploited to study the mechanical behaviour of Topologically Interlocked structures (e.g., Williams and Siegmund 2021; Koureas et al. 2022), also incorporating friction interactions between the fragments. Indeed, such a kind of structures can be understood as a very specific case of "fractured" ones in which the fragment shapes are engineered to obtain a certain mechanical behaviour.

Regarding the available literature specifically aimed at assessing the mechanical behaviour of naturally fractured structures, there can be pointed out the study by Biolzi et al. (2019). In particular, they provided a preliminary estimation of the residual mechanical performance of partially fragmented multilayered glass structures by exploiting the Rigid Body Spring model, initially introduced for masonry structures (Casolo et al. 1999, 2004). This is a heuristic approach which assumes that each fragment is represented by a rigid discrete element whose effective deformation is modelled through the deformation of some interfacial springs which, in turn, also govern the interactions with the surrounding fragments. This allows for a reasonably cheap preliminary modelling of the phenomenon, even in the event of friction, yet at the cost of limiting the analysis to small displacements and unrealistically simple fragment geometries. Likewise, since the interactions between fragments are one-to-one, the computational cost also scales with the number of fragments considered.

Aiming at sorting out some of the drawbacks and limitations showcased by the aforementioned approaches, the present work explores the use of the Phase Field fracture model to predict the residual mechanical performance of fractured domains. Originally introduced by Bourdin et al. (2000) as a theoretically sound regularization of the variational reformulation of brittle fracture by Francfort and Marigo (1998), the Phase Field fracture model exploits the mathematical developments by Ambrosio and Tortorelli (1990) in the field of image segmentation to approximately represent sharp discontinuities as localized transition bands. In doing so, the Phase Field fracture model enriches the displacement problem with a continuous and nonlocally driven scalar field, the so-called phase field, which determines the material soundness and effective stiffness at each point within the domain. This way, cracks are implicitly defined, potentially enabling the numerical representation of any crack pattern, no matter how complex, over any sufficiently refined nonconforming mesh. Of special interest in this regard are the results by Chambolle et al. (2018) and Vicentini et al. (2024), which entail that the Phase Field fracture model can asymptotically replicate unilateral contact conditions with an appropriate selection of the function that modulates the stiffness based on the phase field value. As a result, the Phase Field fracture model emerges as a strong candidate for evaluating the residual behaviour of fractured components, particularly when they are fragmented into multiple and contorted pieces.

2 Review of the Phase Field fracture model theoretical framework

The Phase Field fracture model (PFM) is a variationally consistent and theoretically solid framework for the modelling of fracture events. Rooted in the variational revisitation of brittle fracture by Francfort and Marigo (1998), the PFM cornerstone resides in the principle of

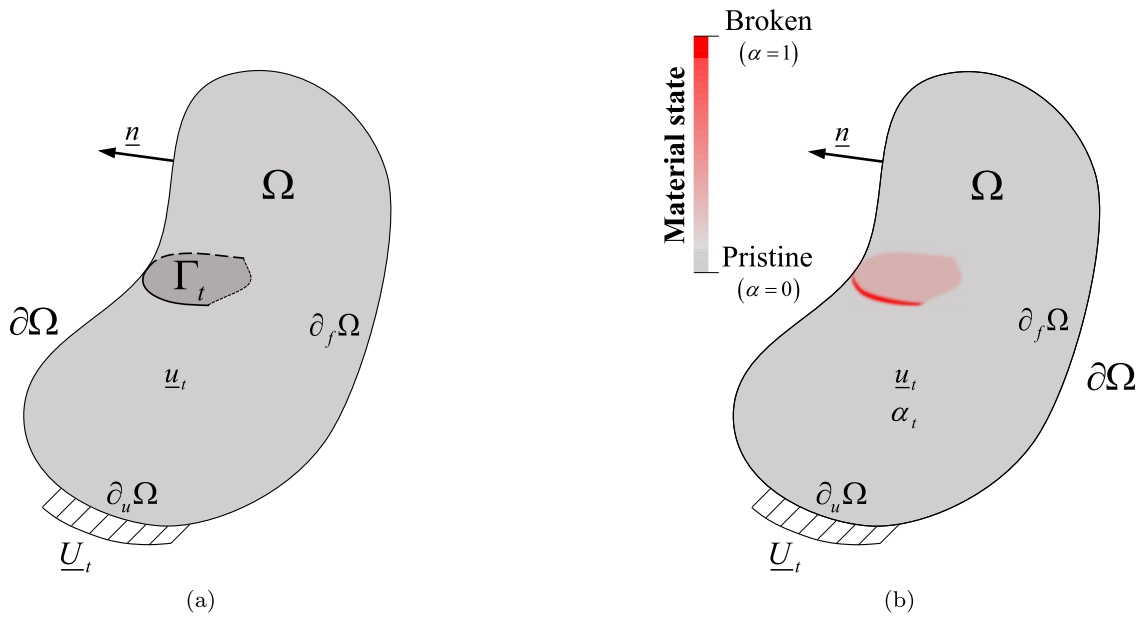


Fig. 1 Schematic representation of: **a** a sharp fracture problem, **b** its PFM representation

minimum potential energy, which is assumed to govern both the deformation state of a structural domain and the topology of the internal cracks. Despite the novelty of this variational paradigm, the discontinuous nature of fracture problems hinders the straightforward numerical implementation for generic scenarios. This limitation was soon overcome by Bourdin et al. (2000), who, inspired by the developments of Ambrosio and Tortorelli (1990), proposed the introduction of a non-locally driven continuous scalar field that governs the material state, the so called *phase field*. Besides giving its name to the framework, this proposal entailed the regularization of the originally discontinuous mechanical problem, rendering it continuous and hence simplifying its numerical implementation.

In order to introduce the PFM's mathematical description in a quasi-static context, let us take the fracture problem illustrated in Fig. 1a, in which a structural domain $\Omega \subseteq \mathbb{R}^N \mid N = \{2,\ 3\}$ of external boundary $\partial\Omega \subseteq \mathbb{R}^N$ and outward normal $\underline{n} : \partial\Omega \rightarrow \mathbb{R}^N$ is subjected to mechanical solicitations while containing an internal sharp crack $\Gamma_t \subseteq \mathbb{R}^N$. Therefore, such a domain deforms per a displacement field $\underline{u} : \Omega \rightarrow \mathbb{R}^N$ that: (i) is continuous anywhere but across Γ_t, and (ii) complies with certain Dirichlet and (homogeneous) Neumann boundary conditions along $\partial_u\Omega$ and $\partial_f\Omega = \partial\Omega \setminus \partial_u\Omega$, respectively. Now, let us omit the existence of Γ_t and enrich the mechanical problem defined in terms of $\underline{u}$ by including the continuous and scalar phase field $\alpha : \Omega \rightarrow [0,\ 1]$, so that $\alpha = 0$ ($\alpha = 1$) represents a pristine (broken) state. This way, the PFM turns continuous the originally discontinuous displacement problem by both regularizing the displacement jumps into localization bands and smearing the sharp crack set Γ_t within the domain Ω (see Fig. 1b). Of course, this requires that $\alpha_t = 1\ \forall \underline{x} \in \Gamma_t$ in addition to any further Dirichlet boundary conditions that might apply over $\partial_\alpha\Omega$.

From an energetic perspective, the system's strain energy $\mathcal{E}_{\text{str}}$ at each instant t is approximated by the PFM as:

$$\mathcal{E}_{\text{str}}\left(\underline{u}_t,\ \alpha_t\right) = \int_\Omega \psi\left(\underline{\underline{\varepsilon}}\left(\underline{u}_t\right),\, a_{\text{PF}}\left(\alpha_t\right)\right)\, \mathrm{d}\underline{x}\,, \tag{1}$$

where the notation $\bullet_t$ represents the magnitude $\bullet$ at the instant t, ψ is the strain energy density modulated by the stiffness modulation function $a_{\text{PF}} : \alpha \rightarrow [0,\ 1]$, and $\underline{\underline{\varepsilon}}\left(\underline{u}\right)$ is the infinitesimal strain tensor defined as:

$$\underline{\underline{\varepsilon}}\left(\underline{u}\right) = \frac{\nabla\underline{u} + \nabla^{\text{T}}\underline{u}}{2}\,. \tag{2}$$

On the other hand, the PFM approximates the system's Griffith fracture energy $\mathcal{E}_{\text{frac}}$ as:

$$\mathcal{E}_{\text{frac}}(\alpha_t) = \int_{\Omega} \frac{G_C}{c_w} \left(\frac{w_{\text{PF}}(\alpha_t)}{\ell} + \ell \, \nabla\alpha_t \cdot \nabla\alpha_t \right) \mathrm{d}\underline{x} \,, \tag{3}$$

where G_C is the specific fracture energy, ℓ is the regularization length and c_w is a scaling coefficient defined in terms of the dissipation function $w_{\text{PF}} : \alpha \to [0,\ 1]$ as:

$$c_w = 4 \int_0^1 \sqrt{w_{\text{PF}}(\alpha)} \, \mathrm{d}\alpha \,. \tag{4}$$

Eventually, in the absence of prescribed body and surface forces, the PFM approximates the system's potential energy $\mathcal{P}$ as:

$$\mathcal{P}\left(\underline{u}_t,\ \alpha_t\right) = \mathcal{E}_{\text{str}}\left(\underline{u}_t,\ \alpha_t\right) + \mathcal{E}_{\text{frac}}(\alpha_t) \,, \tag{5}$$

its local minimization determining the sequence of states $\left(\underline{u}_t,\ \alpha_t\right)$ that the system follows throughout its quasi-static evolution. Of course, this minimization principle is bounded by the admissibility conditions that both $\underline{u}$ and α fields must fulfill anytime. For the former field, admissibility is subjected to the fulfillment of Dirichlet boundary conditions $\underline{u}_t = \underline{U}_t$ over $\partial_u\Omega$; for the latter field instead, admissibility requires not only the fulfillment of Dirichlet boundary condition $\alpha_t = A_t$ over $\partial_\alpha\Omega \cup \Gamma_t$ (with $A_t = 1\ \forall \underline{x} \in \Gamma_t$) but also of the irreversibility condition over α_t. Following conventional procedures of variational calculus, such admissibility conditions can be weakly enforced by requiring that $\underline{u}_t$ and α_t always belong to the affine spaces V_t and B_t defined in Eqs. (6) and (7), respectively.

$$\mathrm{V}_t = \left\{ \underline{u}_t : \Omega \to \mathbb{R}^N \mid \underline{u}_t = \underline{U}_t \ \forall \underline{x} \in \partial_u\Omega \right\} \tag{6}$$

$$\mathrm{B}_t = \left\{ \alpha_t : \Omega \to [0,\ 1] \mid \alpha_t = A_t \ \forall \underline{x} \in \partial_\alpha\Omega \cup \Gamma_t \text{ and } 0 \le \alpha_\tau \le \alpha_t \le 1 \ \forall \underline{x} \times \tau \in \Omega \times [0,\ t) \right\} \tag{7}$$

Furthermore, in order for both $\underline{u}_t + \delta\underline{u}$ and $\alpha_t + \delta\alpha$ to be always admissible, the corresponding variations $\delta\underline{u}$ and $\delta\alpha$ are also subjected to certain admissibility conditions. Particularly, these are weakly enforced by always requiring that $\delta\underline{u} \in \mathrm{V}_0$ and $\delta\alpha \in \mathrm{B}_0$, V_0 and B_0 being the homogeneous counterparts of V_t and B_t, respectively. Thereafter, for any pair of admissible variations $\delta\underline{u}$ and $\delta\alpha$, the first order stability condition of the irreversible system requires that $\delta\mathcal{P} \ge 0$, which after developing writes as:

$$\mathrm{D}_{\underline{u}}\mathcal{P}\left(\underline{u}_t,\ \alpha_t\right)\left[\delta\underline{u}\right] + \mathrm{D}_{\alpha}\mathcal{P}\left(\underline{u}_t,\ \alpha_t\right)\left[\delta\alpha\right] \ge 0 \quad \forall \left\{\delta\underline{u},\ \delta\alpha\right\} \in \{\mathrm{V}_0,\ \mathrm{B}_0\} \,, \tag{8}$$

with $\mathrm{D}_\phi\mathcal{F}(\phi,\ \ldots)\left[\delta\phi\right]$ representing the first Gateaux derivative of the functional $\mathcal{F}$ with respect to the function ϕ and in the direction of the variation $\delta\phi$. It is worth noting that Eq. (8) states that the first-order optimal state is either stationary if the irreversibility condition is not violated ($\delta\mathcal{P} = 0$), or surrounded by higher-energy and inadmissible states ($\delta\mathcal{P} > 0$) if otherwise.

However, as reported by Bourdin et al. (2000), conventional PFM definitions lead to the functional $\mathcal{P}$ not being convex in $\left(\underline{u},\ \alpha\right)$. This means that second order stability considerations are required in order to ascertain that the solution of Eq. (8) is a local minimum (Marigo et al. 2016), hence adding complexity to the problem resolution. However, this burden can be somewhat avoided by exploiting the fact that conventional definitions of $\mathcal{P}$ are convex in both $\left(\underline{u};\ \alpha\right)$ and $\left(\alpha;\ \underline{u}\right)$, with the semicolon separating variables on its left from fixed parameters on its right. This allows for iteratively approaching the local minimum of $\mathcal{P}$ by alternate resolution of the two staggered first-order minimization principles, one for $\underline{u}_t$ (at a given α):

$$\mathrm{D}_{\underline{u}}\mathcal{P}\left(\underline{u}_t;\ \alpha\right)\left[\delta\underline{u}\right] = 0 \ \forall\delta\underline{u} \in \mathrm{V}_0 \,, \tag{9}$$

and another one for α_t (at a given $\underline{u}$):

$$\mathrm{D}_{\alpha}\mathcal{P}\left(\alpha_t;\ \underline{u}\right)\left[\delta\alpha\right] \ge 0 \ \forall\delta\alpha \in \mathrm{B}_0 \,. \tag{10}$$

Now, substituting $\mathcal{P}$ by its definition in terms of the strain and fracture energy from Eqs. (1) and (3) and developing the Gateaux derivatives, one obtains the following weak form for the displacement problem:

$$\int_{\Omega} \frac{\partial\psi\left(\underline{\underline{\varepsilon}}\left(\underline{u}_t\right);\ a_{\text{PF}}(\alpha)\right)}{\partial\underline{\underline{\varepsilon}}} : \underline{\underline{\varepsilon}}\left(\delta\underline{u}\right) \mathrm{d}\underline{x} = 0 \ \forall\delta\underline{u} \in \mathrm{V}_0 \,, \tag{11}$$

with $\partial\psi/\partial\underline{\underline{\varepsilon}}$ being the dual magnitude of $\underline{\underline{\varepsilon}}$, also known as the stress tensor $\underline{\underline{\sigma}}$. Likewise, the developed governing principle for α reads as:

$$\int_{\Omega} \frac{G_C}{c_w} \left(\frac{1}{\ell} \frac{\partial w_{\text{PF}}(\alpha_t)}{\partial\alpha} \delta\alpha + 2\ell \, \nabla\alpha_t \cdot \nabla\delta\alpha \right) \mathrm{d}\underline{x} + + \int_{\Omega} \frac{\partial\psi\left(a_{\text{PF}}(\alpha_t);\ \underline{\underline{\varepsilon}}\left(\underline{u}\right)\right)}{\partial\alpha} \delta\alpha \, \mathrm{d}\underline{x} \ge 0 \ \forall\delta\alpha \in \mathrm{B}_0 \,, \tag{12}$$

where $\partial\psi/\partial\alpha$ is commonly referred to as the crack driving force. It is worth noting that the variational principle in Eq. (11) enforces the domain Ω to be in quasi-static equilibrium of forces provided a stiffness distribution governed by α. On the other hand, Eq. (12)

can be understood as a damage criterion that drives the development of α (or lack thereof) provided a state of deformation $\underline{u}$. Of course, the fixed parameters in each of the staggered variational principles must correspond to their corresponding best guesses available. Therefore, the staggered PFM is essentially analogous to a multi-physics problem that couple two physical sub-problems: one mechanical and one fracture-wise.

3 The Phase Field approach for assessing the mechanical behaviour of fractured media

Ever since its inception, the PFM has been extensively exploited to model the nucleation and evolution of fracture in domains subjected to certain loading conditions. In contrast to this, the present work pursues another approach and seeks to investigate the PFM's capability to describe the residual mechanical performance of already broken domains for which the sharp crack pattern $\Gamma_0 = \Gamma$ is known. This way, the proposed methodology can benefit from the theoretically rigorous implicit definition of cracks that characterizes the PFM, in turn allowing the study of arbitrarily complex crack patterns over a non-conforming domain discretization. In such a way, the interaction between crack lips is implicitly managed by the PFM, hence avoiding the complex implementation of conventional discrete crack modelling techniques, which require to explicitly define each of the existing contact pairs or interfacial interactions.

To that end, it is first required to determine the field α that approximates the known crack set Γ in the absence of mechanical solicitations, i.e. for $\underline{u} = \underline{0}$. From a continuum standpoint, this essentially consists in solving the variational principle in Eq. (12) assuming that $\partial\psi/\partial\alpha = 0$ and $\alpha = 1 \ \forall \underline{x} \in \Gamma$. Nonetheless, the latter boundary condition does not hold its robustness upon a Finite Element (FE) implementation since the discretization procedure involves the element-wise determination of the effective properties, and Γ is an $N-1$-dimensional locus of points (see Fig. 2a). As such, the sought after lack of stiffness in the presence of a crack can only be reproduced by the PFM if $\alpha = 1$ is true within a stripe $\Omega_\Gamma \subseteq \mathbb{R}^N$ that contains whole elements surrounding Γ. In particular, provided that the finite elements have a characteristic size equal to h_Γ in the surroundings of Γ, Ω_Γ can be defined as the $\xi\, h_\Gamma -$ neighbourhood of Γ depicted in Fig. 2b. Mathematically, the definition of such a geometrical locus writes as:

$$\Omega_\Gamma = \left\{ \underline{x} \in \Omega \;\middle|\; \mathrm{d}\left(\underline{x},\, \Gamma\right) \leq \xi\, h_\Gamma \right\} , \tag{13}$$

where $\mathrm{d}\left(\underline{x},\, \Gamma\right)$ represents the minimum distance of a point $\underline{x}$ to Γ, and $\xi > 1$ is a scaling parameter governing the extension of Ω_Γ as a multiple of h_Γ. Given this, the affine space B_t of admissible α fields can be substituted upon FE implementation by $\hat{\mathrm{B}}_t$, in turn defined as:

$$\hat{\mathrm{B}}_t = \Big\{ \alpha_t : \Omega \to [0,1] \,|\, \alpha_t = 1 \ \forall \underline{x} \in \Omega_\Gamma \text{ and } 0 \leq \alpha_\tau \leq \alpha_t \leq 1 \ \forall \underline{x} \times \tau \in \Omega \times [0,t) \Big\} , \tag{14}$$

which in the $\xi\, h_\Gamma \to 0$ limit reverts to B_t from Eq. (7) after assuming that $\partial_\alpha \Omega = \varnothing$. The irreversibility condition for α is retained in Eq. (14) as a vestige of the conventional PFM definition, yet it is not required for the present approach since α is kept constant throughout the mechanical loading. As such, α results to not be herein associated with any instant t in particular, and so its subindex t will be hereafter dropped to emphasize its constant nature for a given Ω_Γ. Hence, taking the staggered variational principle in Eq. (12) and setting $\underline{u} = \underline{0}$, the governing principle for the α field approximating the known fractured state Γ particularizes as:

$$\int_\Omega \frac{1}{\ell} \frac{\partial w_{\mathrm{PF}}(\alpha)}{\partial \alpha} \delta\alpha + 2\ell\, \nabla\alpha \cdot \nabla\delta\alpha \, \mathrm{d}\underline{x} \geq 0 \ \forall \delta\alpha \in \hat{\mathrm{B}}_0 , \tag{15}$$

where now $\hat{\mathrm{B}}_0$ represents the homogeneous counterpart of $\hat{\mathrm{B}}_t$. The resolution of Eq. (15) yields the continuously defined α field that smears Ω_Γ within Ω. Consequently, the resolution of Eq. (15) will also be hereafter referred to as the diffusion of α. Known α, the resolution of the variational principle in Eq. (11) then allows to determine the corresponding $\underline{u}$ field for the given fracture pattern and prescribed loading and boundary conditions. Remarkably, it results that the staggering resolution procedure, which is commonly used to approximate the solution to the PFM's monolithic variational principle, somewhat reveals itself to be the rigorous regularized modelling of the actual physical phenomenon herein.

At this point, it only remains to define the particular functions that govern the mechanical behaviour in terms of the $\underline{u}$ and α fields, viz. ψ, a_{PF} and w_{PF}. Regarding the two latter, the so-called AT1 model introduced

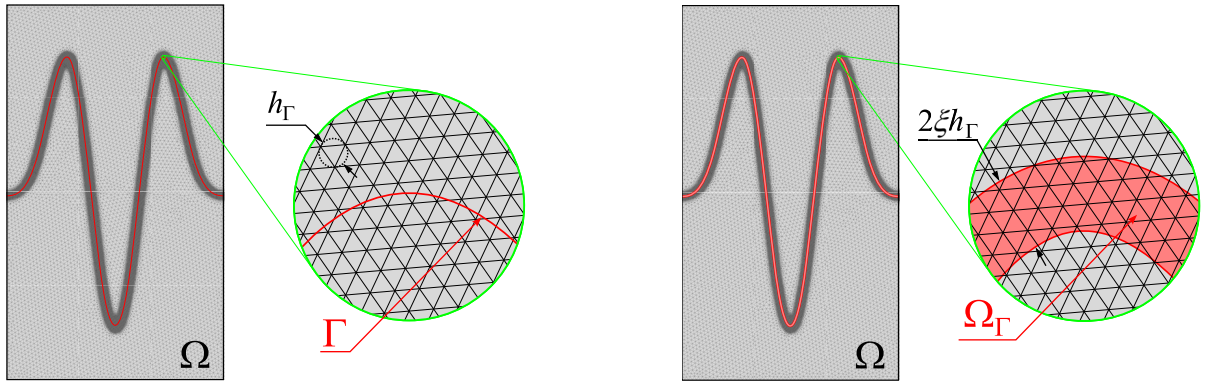


Fig. 2 Schematic representation of a spatially discretized 2D domain overlaid with: **a** a 1-dimensional crack set Γ_t and **b** the corresponding 2-dimensional geometrical locus Ω_Γ defined in Eq. (13)

by Pham et al. (2011) will be hereafter used, this consisting in:

$$\text{AT1}: \begin{cases} a_{\text{PF}}(\alpha) = (1-\alpha)^2 + k \\ w_{\text{PF}}(\alpha) = \alpha \\ c_w = \dfrac{8}{3} \end{cases} \tag{16}$$

with k representing a small parameter ($k << 1$) that avoids numerical instabilities when $\alpha \to 1$. This choice is mainly motivated by AT1's ability to yield small-supported α fields, i.e. so that $\alpha > 0$ only in the vicinity of Ω_Γ, while presenting a reasonably simple mathematical definition.

On the other hand, the α-modulated strain energy density function ψ must ideally satisfy two conditions: (i) that no tensile nor shear tractions can be transmitted through cracks, and (ii) that compressive stresses must be transmissible across cracks as in the case of pristine conditions, in order to prevent the crack lips from interpenetrating into each other. Such a behaviour is achieved by introducing the dependency of the mechanical response on α through the so-called strain energy decomposition, of which many different options are available in the literature (see e.g. De Lorenzis and Maurini 2022). Nonetheless, among all these, the Cleavage–Deviatoric split proposed by Amor et al. (2009) is a reasonably simple and well-established choice that can fulfill all the aforementioned requisites, although it only does so exactly in the sense of Γ-convergence (Vicentini et al. 2024). Therefore, in order for the proposed approach to still retrieve the sharp crack limit as $\ell \to 0$, the thickness of Ω_Γ is ought to be proportional to ℓ, i.e. $\xi h_\Gamma \propto \ell$. On the downside, the Cleavage–Deviatoric split has been proven to feature some spurious effects upon the unconfined lateral expansion of cracked regions (see e.g. Steinke and Kaliske 2019), and so the simplicity of this modeling choice comes at the cost of limiting the proposed approach to laterally confined specimens under compression. It is to be noted, however, that this limitation is not intrinsic to the proposed PFM-based approach but to the chosen energy decomposition, and this can be overcome by using more intricate and complex choices such as the directional split (Strobl and Seelig 2015; Fei and Choo 2019; Steinke and Kaliske 2019). Nonetheless, for the sake of simplicity, let us stick to the Cleavage–Deviatoric split in what follows.

3.1 Cleavage–Deviatoric strain energy decomposition

Generally speaking, the PFM's strain energy split divides ψ into a damageable term ψ_D affected by α, and an α-independent residual term ψ_R. Their specific definitions end up determining the interaction between the mechanical and fracture aspects of the PFM, since these modulate the effect that α have on ψ for a certain $\underline{u}$. In particular, by separating the mechanical and fracture inputs of ψ, i.e. $\underline{\underline{\varepsilon}}$ and a_{PF}, such a split can be mathematically expressed in a generic fashion as:

$$\psi\left(\underline{\underline{\varepsilon}}, a_{\text{PF}}\right) = a_{\text{PF}}\ \psi_D\left(\underline{\underline{\varepsilon}}\right) + \psi_R\left(\underline{\underline{\varepsilon}}\right) . \tag{17}$$

For the particular case of a linear elastic material whose pristine strain energy density is given by:

$$\psi_0\left(\underline{\underline{\varepsilon}}\right) = \frac{\lambda}{2}\text{tr}\left(\underline{\underline{\varepsilon}}\right)^2 + \mu\left(\underline{\underline{\varepsilon}} : \underline{\underline{\varepsilon}}\right) , \tag{18}$$

with λ and μ being the material's Lamé constants, the Cleavage–Deviatoric energy split proposed by Amor et al. (2009) defines the corresponding ψ_D^{CD} and ψ_R^{CD} terms as:

$$\psi_D^{\mathrm{CD}}\left(\underline{\underline{\varepsilon}}\right) = \left[\left(\frac{\lambda}{2}+\frac{\mu}{3}\right)\mathrm{tr}^{+}\left(\underline{\underline{\varepsilon}}\right)^2 + \mu\left(\underline{\underline{\varepsilon}}_{\mathrm{dev}} : \underline{\underline{\varepsilon}}_{\mathrm{dev}}\right)\right], \tag{19}$$

$$\psi_R^{\mathrm{CD}}\left(\underline{\underline{\varepsilon}}\right) = \left(\frac{\lambda}{2}+\frac{\mu}{3}\right)\mathrm{tr}^{-}\left(\underline{\underline{\varepsilon}}\right)^2, \tag{20}$$

where $\mathrm{tr}^{\pm}\left(\underline{\underline{\varepsilon}}\right) = \left(\mathrm{tr}\left(\underline{\underline{\varepsilon}}\right) \pm \left|\mathrm{tr}\left(\underline{\underline{\varepsilon}}\right)\right|\right)/2$, and $\underline{\underline{\varepsilon}}_{\mathrm{dev}}$ represents the deviatoric part of $\underline{\underline{\varepsilon}}$, which, representing the identity tensor as $\underline{\underline{I}}$, gets defined as follows:

$$\underline{\underline{\varepsilon}}_{\mathrm{dev}} = \underline{\underline{\varepsilon}} - \frac{1}{3}\mathrm{tr}\left(\underline{\underline{\varepsilon}}\right)\underline{\underline{I}}. \tag{21}$$

Therefore, it becomes clear from Eqs. (17), (19) and (20) that the deformations yielding deviatoric and/or positive volumetric terms do not carry an increase of strain energy when $\alpha = 1$. In contrast, those only featuring negative volumetric terms maintain their energetic contribution regardless of α. Moreover, the split of the strain energy density into the damageable and residual terms leads to an analogous decomposition in the stress tensor $\underline{\underline{\sigma}}$ which can be mathematically expressed as:

$$\underline{\underline{\sigma}}^{\mathrm{CD}}\left(\underline{\underline{\varepsilon}},\, a_{\mathrm{PF}}\right) = a_{\mathrm{PF}}\,\underline{\underline{\sigma}}_D^{\mathrm{CD}}\left(\underline{\underline{\varepsilon}}\right) + \underline{\underline{\sigma}}_R^{\mathrm{CD}}\left(\underline{\underline{\varepsilon}}\right), \tag{22}$$

with the damageable $\underline{\underline{\sigma}}_D^{\mathrm{CD}}$ and residual $\underline{\underline{\sigma}}_R^{\mathrm{CD}}$ stress tensors being defined as follows:

$$\underline{\underline{\sigma}}_D^{\mathrm{CD}}\left(\underline{\underline{\varepsilon}}\right) = \left(\lambda + \frac{2\mu}{3}\right)\mathrm{tr}^{+}\left(\underline{\underline{\varepsilon}}\right)\underline{\underline{I}} + 2\mu\,\underline{\underline{\varepsilon}}_{\mathrm{dev}}, \tag{23}$$

$$\underline{\underline{\sigma}}_R^{\mathrm{CD}}\left(\underline{\underline{\varepsilon}}\right) = \left(\lambda + \frac{2\mu}{3}\right)\mathrm{tr}^{-}\left(\underline{\underline{\varepsilon}}\right)\underline{\underline{I}}. \tag{24}$$

4 Effect of ℓ on the resultant crack lips interaction

As stated by Vicentini et al. (2024), the Cleavage–Deviatoric energy split can perfectly mimic unilateral contact interactions between the crack lips only in the sense of Γ-convergence, i.e. for $\ell \to 0$. At the same time, the regularization nature of the PFM also supports seeking such a limit because it leads to retrieving the original sharp problem. However, in the event of implementing the PFM in an FE context, the $\ell \to 0$ limit can only be pursued at a prohibitive computational cost since the $\ell/h > 1$ condition must be met at least in the vicinity of Ω_Γ. Moreover, given that the PFM regularizes the sharp discontinuities into transition bands of width proportional to ℓ, making $\ell \to 0$ results in fields whose gradients' L2-norm might tend to infinity, hence potentially jeopardizing the use of numerical resolution methods. Therefore, exploiting the PFM to assess the mechanical performance of already broken domains requires finding a delicate compromise in the choice of ℓ, so that it is sufficiently small to yield accurate predictions yet large enough to be numerically manageable. In this regard, the present section reports a series of case studies that aim to shed some light into the actual effect that changing the magnitude of ℓ has on the accuracy of the PFM-based approach for the structural assessment of fractured media.

The subsequent case studies exploiting the PFM-based approach were implemented using the open source Finite Element library FEniCSx (Alnaes et al. 2015; Baratta et al. 2023) in a Python environment. For the sake of simplicity, all simulations were performed under plane strain conditions, and so $N = 2$. Likewise, the domain discretization was done with first order triangular elements whose characteristic size h_Γ is at most equal to $\ell/4$ in the regions where it is expected that $\alpha > 0$, hence following conventional PFM modeling choices (see e.g. Bleyer et al. 2017). Everywhere else, coarser meshes were used in order to reduce the computational cost of the simulations, yet this was found to hardly affect the simulation results. Moreover, in order to retain the PFM's regularization nature, Ω_Γ will be hereafter defined as the $\ell/2$-neighbourhood of Γ, i.e. $\xi \geq 2$ herein since $4h_\Gamma \leq \ell$. In order to allow an algorithmically efficient construction of the numerical model regardless of the complexity of Γ, the definition of Ω_Γ and the associated element size distribution will be optically encoded following the procedure defined in Appendix A. Eventually, the lack of an inherent size-effect in the governing principles in Eqs. (11) and (15) allows to conduct the dimensional analysis in a normalized fashion. As such, the ensuing numerical simulations used $E = 1.0$ $\left[\mathrm{Force/Length}^2\right]$ and $\nu = 0.2$ $[-]$, with E and ν being the Young's modulus and Poisson's ratio, respectively.

For the sake of validation, the considered case studies whose exact solution is not trivial, i.e. case studies B and C, are also solved in Ansys Mechanical by using hard and frictionless contact interactions between the fragments. Algorithmically, these are enforced using a penalty approach with a stiffness

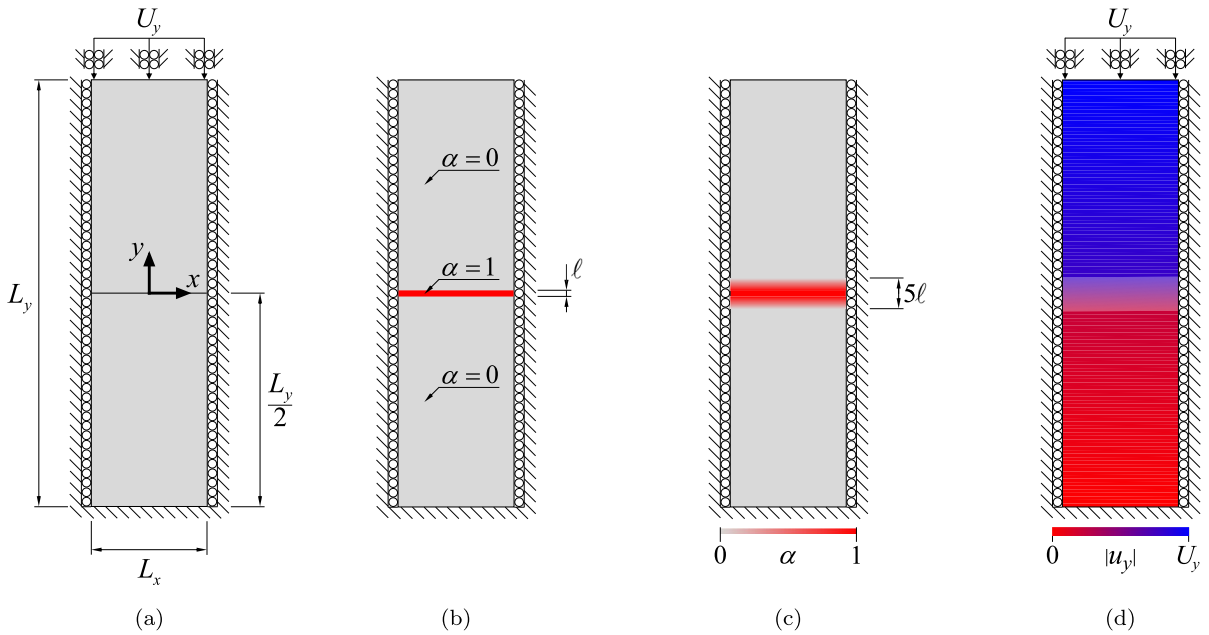


Fig. 3 Illustration of: **a** a domain with effectively infinite width subjected to confined vertical compression and containing a centered horizontal crack; and the corresponding PFM approximation **b** before and **c** after diffusing α under $\underline{u} = \underline{0}$ and **d** upon the vertical confined compression test

of $k_{pen} = 5 \cdot 10^5 \left[\text{Force/Length}^3\right]$ so as to ensure that the obtained contact interpenetration remains several orders of magnitude smaller than the obtained displacements.

4.1 Case study A: Confined domain with a single horizontal crack

The first case study carried out involves the scenario illustrated in Fig. 3a, where a rectangular bidimensional domain of dimensions $L_x \times L_y$: (i) is laterally confined in order to mimic an infinite width, (ii) contains a centered horizontal crack, and (iii) is subjected to vertical uni-axial compression by an imposed displacement equal to U_y over the upper edge. Given these characteristics, the problem results pseudo-onedimensional in that it is independent from the spatial coordinate x. This implies that the only non-null component of the strain tensor $\underline{\underline{\varepsilon}}$ is ε_{yy}, thereby rendering this setup the simplest for testing the PFM's ability to reproduce the compressive non-interpenetration across a crack. To that end, it is here introduced a nominal vertical stiffness measure K_y, whose definition is:

$$K_y = \frac{F_y}{L_x}\frac{L_y}{U_y}\,, \tag{25}$$

with F_y being the resultant reaction force (per unit of thickness) applied along the upper edge. Of course, K_y is a structural property which, for the case at hand, remains constant regardless of L_x since $F_y \propto L_x$. Moreover, $K_y = \lambda + 2\mu = K_{y0}$ for a pristine domain, which is also true when considering perfect unilateral contact interactions between the crack lips for the given setup. On the other hand, should α be homogeneous within Ω and equal to 1, the stiffness measure would be $K_y = \lambda + 2\mu/3 = K_{y1}$ per the Eq. (24). As such, provided that $\lambda = 5/18 \left[\text{Force/Length}^2\right]$ and $\mu = 5/12 \left[\text{Force/Length}^2\right]$, the PFM's residual stiffness predictions get here more accurate as $K_y/K_{y1} \to K_{y0}/K_{y1} = 2$. Remarkably, the homogeneous nominal stiffness K_{y1} is independent of the imposed crack pattern, and so it will be hereinafter used to report the obtained nominal vertical measures in a normalized fashion through the K_y/K_{y1} ratio.

The procedure for implementing the PFM-based approach is illustrated in Fig. 3b–d. This essentially consists in first identifying the subdomain Ω_Γ that corresponds to the $\ell/2$-neighbourhood of the centered hor-

izontal crack, wherein $\alpha = 1$ is set; everywhere else it remains that $\alpha = 0$ (see Fig. 3b) yet this condition is not enforced thereafter. Using this binary distribution of α as an initial guess, Eq. (15) is numerically solved to diffuse α within the domain, yielding the continuous distribution illustrated in Fig. 3c. Since the considered problem is monodimensional and the AT1 model is used, α is smeared throughout a compact band whose thickness is increased by 4ℓ with respect to Ω_Γ's (see e.g. Marigo et al. 2016). The PFM approximation of the displacement field $\underline{u}$ is then obtained as in Fig. 3d by numerically solving the variational principle in Eq. (11) with the provided mechanical boundary conditions. Eventually, the resultant K_y is determined by post-processing the results from the mechanical problem. Repeating this whole process for several values of ℓ/L_y ranging from $\ell/L_y \sim 10^{-3}$ to $\ell/L_y \sim 10^{0}$ yields the K_y/K_{y1} results reported in Fig. 4. From these, it is evident that very small values of ℓ/L_y allow the PFM to approach the sought after $K_y/K_{y1} = 2$, with $\ell/L_y \approx 0.01$ already yielding a practical-wise admissible $K_y/K_{y1} \approx 1.94$. In contrast, when $\ell/L_y \to 1$, the PFM problem approximates to the $\alpha = 1$ homogeneous case, and so $K_y/K_{y1} \to 1$.

Remarkably, given the boundary conditions chosen for this case study, the obtained results do not only apply for the case of a single horizontal crack in the domain, but also to those in which there are n horizontal cracks vertically stacked and evenly spaced. For such cases, the plot in Fig. 4 remains unvaried once the magnitude reported in the horizontal axis is generalized from ℓ/L_y to $(n+1)\,\ell/2L_y$.

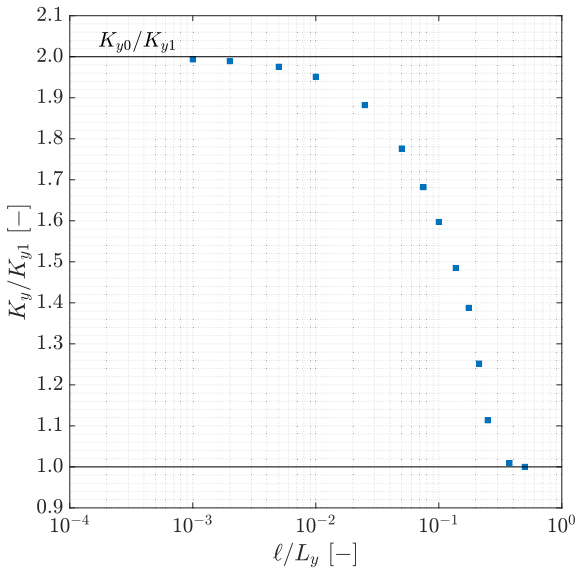


Fig. 4 Effect of ℓ/L_y on K_y/K_{y1} resulting from a confined domain with a single horizontal crack

4.2 Case study B: Confined domain with a single straight piecewise inclined crack

The second case study here addressed involves a straight piecewise inclined crack as shown in Fig. 5a. For all the ensuing simulations, the following characteristic dimensions are used: $L_x = 0.27$ [Length], $L_y = 1$ [Length] and $\epsilon = 0.01$ [Length]; as well as three different crack inclinations corresponding to $\varphi = \{30,\ 45,\ 60\}°$. Please notice that the presence of horizontal crack segments at the intersections with the lateral boundaries is motivated by the no-flux boundary condition in force for α, which mathematically writes as $\nabla\alpha \cdot \underline{n} = 0\ \forall \underline{x} \in \partial\Omega$ (see e.g. Kumar et al. 2020). As such, the PFM as a whole can only deal with smeared cracks that are "perpendicular" to $\partial\Omega$; any crack Γ not complying with this condition cannot be regularized by a phase field α from a strictly rigorous standpoint. Therefore, given that the conducted analysis stands on the ground of the PFM's Γ-convergence, all the studied crack topologies are perpendicular to the domain boundaries. The obtained PFM results in terms of the K_y/K_{y1} ratio for the different values of φ and ℓ/L_y are reported in Fig. 5b, along with the corresponding predictions by the contact-based Ansys model K_y^{FE}/K_{y1}. From these results, it becomes evident that larger values of φ require smaller ℓ/L_y ratios in order for the PFM-based approach to yield results close to the contact-based benchmark. A possible explanation for this effect lies in that the minimum characteristic length of the fragments gets smaller as φ gets larger, hence undermining the accuracy of the results by virtue of the Γ-convergence. Likewise, it was observed that the relative sliding at the interface between fragments entailed the necessity of more refined meshes in the vicinity of Ω_Γ so as to ensure acceptable mesh-independence of the results. For complete disclosure, results in Fig. 5b correspond to a mesh whose refined elements have a characteristic length at most equal to $\ell/8$, which was determined via a parametric analysis to yield reasonably mesh-independent results. In comparison, results in Fig. 4 were obtained with refined elements with a characteristic length equal to $\ell/4$ at most.

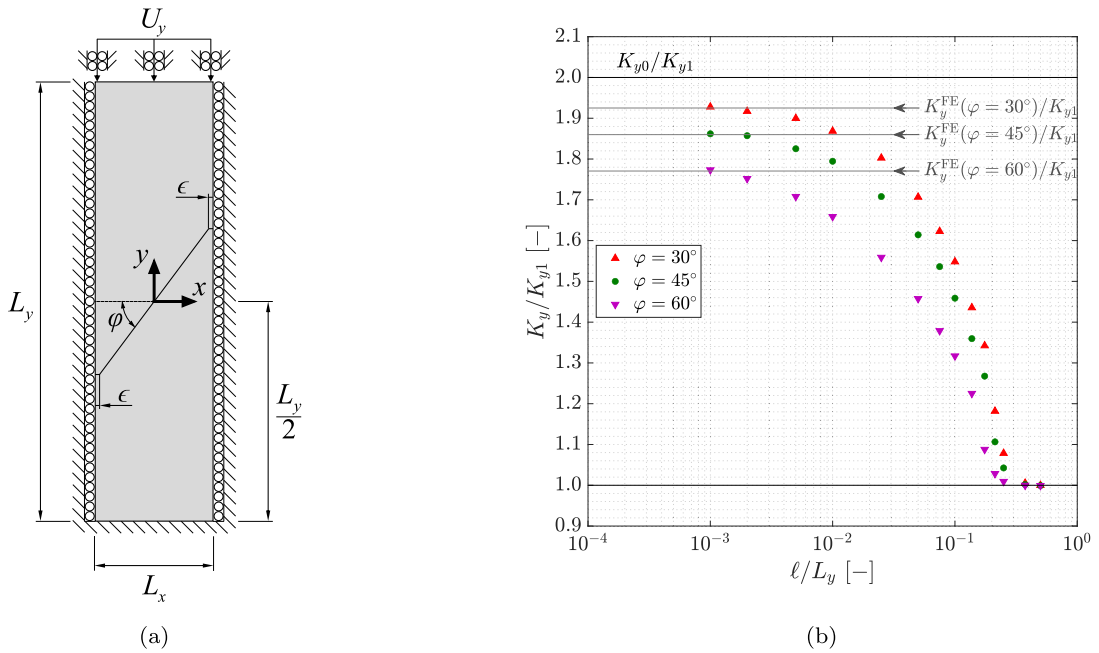


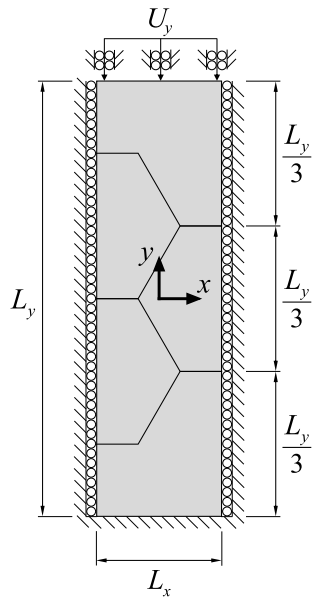
Fig. 5 Effect of ℓ/L_y on K_y/K_{y1} with φ as a parameter resulting from confined domains with a single straight piecewise inclined crack

4.3 Case study C: Confined domain with honeycomb crack patterns

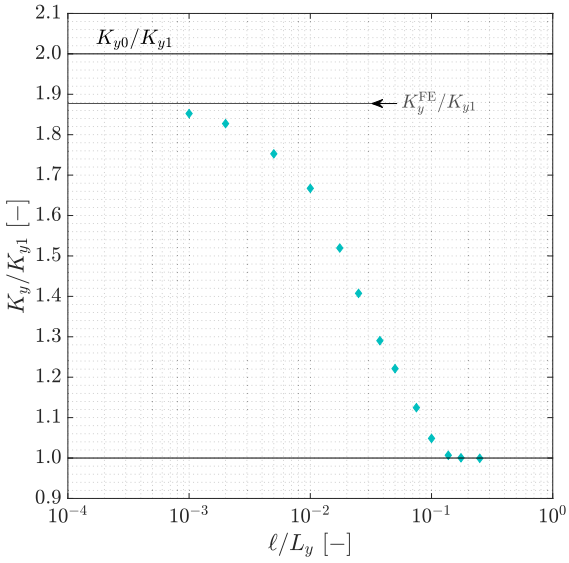
The last case study here conducted involves the honeycomb-like multi-fragmented domain under confined compression that is illustrated in Fig. 6a. The overall domain dimensions for this case study are $L_x = 1/\left(2\sqrt{3}\right)$ [Length] and $L_y = 1$ [Length], whereas each of the three central fragments is half a regular hexagon whose apothem is $L_y/6$. Per the observations made in the previous subsection regarding the necessity of smaller elements in the presence of inclined crack segments, the mesh is also here refined in the surroundings of Ω_Γ to showcase elements with a characteristic length no larger than $\ell/8$.

The obtained PFM predictions in terms of the K_y/K_{y1} ratio for various values of ℓ/L_y are reported in Fig. 6b, as well as the contact benchmark result K_y^{FE}/K_{y1} from the corresponding Ansys model. In line with previous observations, the PFM predictions do converge to K_y^{FE}/K_{y1} as the ℓ/L_y ratio tends to zero, yet at a slower rate. This difference can be explained by a smaller minimum fragment size for the case at hand, which is equal to $L_y/6 \approx 0.167L_y$, as opposed to the approximate value of $0.28L_y$ for $\varphi = 60°$ in the previous subsection, for instance. Therefore, from these results one can state that the PFM's regularization length ℓ must be sufficiently small in comparison with the characteristic length of both the domain and fragments.

While conducting the simulations that yielded the above mentioned results, it was observed that the combination of more complex crack patterns with small values of ℓ/L_y resulted in worse convergence rates for the numerical solvers. A detailed analysis of the obtained solutions revealed that the main culprit for this loss of solver effectiveness was the presence of some spurious deformations observed within Ω_Γ in the surroundings of crack vertices. This is in line with the divergence issues already observed by Steinke and Kaliske (2019) upon unconfined compression of completely cracked domains. Additional analyses also showed that such distortions were stronger the more elements where within Ω_Γ, hence posing a topic to be further investigated in future studies. Moreover, these localized phenomena were observed to have a slight effect on the displacement field, especially on its horizontal component u_x (see Fig. 7b). These results infer the need of further modifying the definition of the strain energy decomposition so as to robustly deal with cracks show-



(a)



(b)

Fig. 6 Effect of ℓ on the K_y/K_{y1} ratio resulting from confined domains with a honeycomb crack pattern

casing sharp angles. Nonetheless, the overall effect of these distortions was deemed negligible, since the primary displacement component, i.e. u_y, presents great agreement with respect to the contact-based benchmark model, as shown in Fig. 7c, d. Remarkably, the results therein reported imply that the agreement between the two models is not only qualitative but also quantitative, hence undeniably supporting the validity of the proposed PFM-based approach for characterizing the residual structural performance of fractured media.

5 Conclusions and future outlook

This work explores a novel approach for characterizing the residual structural performance of fractured media on the basis of the well-established Phase Field fracture model (PFM). To that end, the conventional staggered resolution of the PFM's variational principle is fully exploited: first, the continuous distribution of the phase field α for the known crack pattern Γ is determined in the absence of mechanical solicitations; and then, the domain is mechanically loaded and the displacement field $\underline{u}$ is obtained for the given α. In this latter part, the interaction between the different fragments is implicitly managed by the PFM formulation by means of the Cleavage–Deviatoric strain energy decomposition. This choice allows the proposed approach to rely on a theoretically rigorous definition of the unilateral contact interactions across cracks. Furthermore, the use of a phase field to implicitly define the crack topology and the interactions between the crack lips eliminates the necessity for explicit definition of the contact pairs, hence posing a great computational advantage in the event of massively-fragmented domains. In addition to introducing the basic theoretical and procedural aspects of the approach, this work has also reported its application to three different case studies on the effect that the regularization length has on the approach accuracy. For each of the non-trivial fragmenting patterns here considered, a contact-based Ansys model was also implemented as a mean of validation. Remarkably, the proposed approach showed great agreement with each of the corresponding benchmark results, thus proving its robustness and representativeness.

Despite its promising outlook and novelty, the as-is proposed PFM-based approach still faces some challenges and limitations relevant to its practical use. For instance, the Cleavage–Deviatoric's necessity of very small regularization lengths by virtue of the Γ-convergence also involves Finite Element models with very refined discretizations; although these are only required in very localized and *a priori* known regions. Therefore, the implementation of more advanced meshing procedures able to deal with extreme element

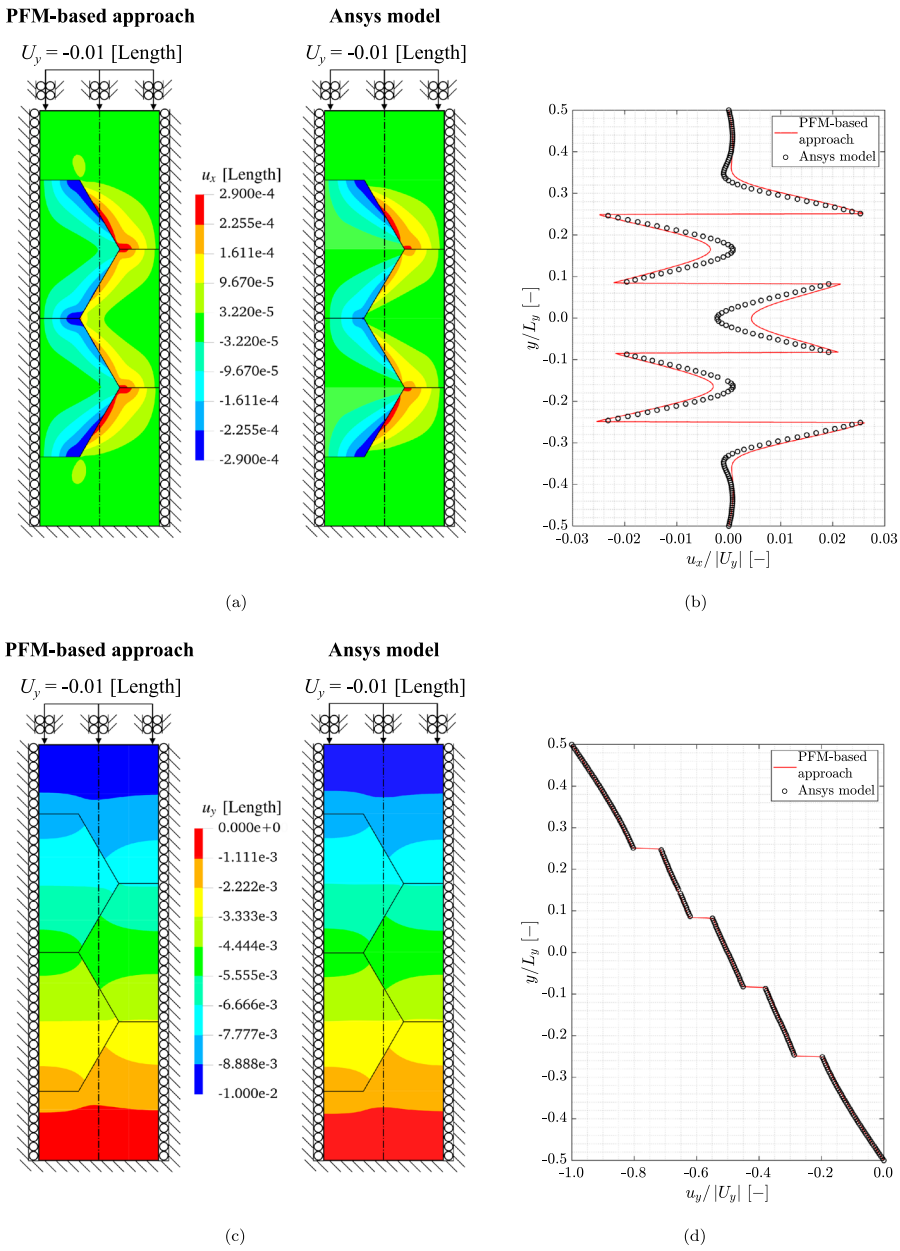


Fig. 7 Confined domain with a honeycomb crack pattern: normalized contour plots for **a** u_x and **c** u_y; normalized evolution of **b** u_x and **d** u_y over the $x = 0$ line (dashdotted line over the contour plots). The PFM results correspond to $\ell/L_y = 10^{-3}$

refinements is paramount herein. Likewise, the results reported in the last case study clearly evidence that the Cleavage–Deviatoric strain energy decomposition is not universally robust nor intrinsically accurate for representing non-interpenetration interactions upon unconfined compression states, in line with the findings already reported by Steinke and Kaliske (2019). Therefore, further developments of the PFM-based approach here introduced will require implementing more complex and adequate strain energy decompositions, such as the directional split (Steinke and Kaliske 2019). In this regard, the technique proposed in Appendix A for optically encoding modelling information could be exploited to declutter the spatial definition of the *a priori* known local crack orientation system, hence considerably streamlining an otherwise unfathomable approach. On another note, given that the approach approximates discontinuities while remaining in a continuum setup, its application is limited to cases in which the sliding and relative movements between the frag-

ments are small. Nonetheless, there are many cases of practical relevance for which this condition still applies, such as the post-partial-fracture characterization of laminated glass components (see e.g. Veer et al. 2008; Angelides et al. 2022; Corrado et al. 2024). For scenarios in which the fragment displacements are large instead, another relevant yet radically different Phase-Field-based approach was recently proposed by Lorez et al. (2024) within a Eulerian Framework. Therefore, a prospective line of research is to delve into the similarities and differences of these approaches, so as to elucidate about their respective advantages, limitations and even synergies. Finally, future studies could be oriented towards exploring how crack propagation can be incorporated into the proposed PFM-based approach in a theoretically rigorous manner, hence allowing it to reconcile with the scope of conventional Phase Field models of fracture. Nonetheless, in order to successfully manage such an extension of the PFM-based approach, there are some crucial theoretical aspects that should be addressed beforehand. These include, for instance, how to properly deal with crack nucleation within a PFM framework (see e.g. Kumar et al. 2020; Lopez-Pamies et al. 2025), and the observance of dynamic effects upon unstable fracture in the presence of energetic barriers (see e.g. Chao Correas et al. 2024).

Acknowledgements This project has received funding from the European Union's Horizon 2020 research and innovation programme under the Marie Skłodowska Curie Grant Agreement No. 861061

Funding Open access funding provided by Politecnico di Torino within the CRUI-CARE Agreement.

Declarations

Conflict of interest The authors declare that they have no conflict of interest.

Open Access This article is licensed under a Creative Commons Attribution 4.0 International License, which permits use, sharing, adaptation, distribution and reproduction in any medium or format, as long as you give appropriate credit to the original author(s) and the source, provide a link to the Creative Commons licence, and indicate if changes were made. The images or other third party material in this article are included in the article's Creative Commons licence, unless indicated otherwise in a credit line to the material. If material is not included in the article's Creative Commons licence and your intended use is not permitted by statutory regulation or exceeds the permitted use, you will need to obtain permission directly from the copyright holder. To view a copy of this licence, visit http://creativecommons.org/licenses/by/4.0/.

Appendix A: Algorithmically-efficient technique for optically encoding modelling information

This appendix describes the technique used for efficiently prescribing complex field distributions on a Finite Element model through digital-optical encoding. The cornerstone of this approach lies in the raster map behind every digital image, which is a data structure that stores point-wise discrete numerical values corresponding to certain positions in space within a uniformly spaced array, also known as pixels. Each raster map is hence associated to a certain structured and homogeneous spatial discretization, and so it can be easily mapped to a Finite Element mesh if both represent the same geometrical domain. Therefore, the information stored in each pixel can be used to encode modelling information to be passed to the corresponding element nodes and integration points.

In this work, such a paradigm was for instance exploited for imposing $\alpha = 1$ within Ω_Γ through the procedure illustrated in Fig. 8. To that end, Inkscape v1.3.2 (2023) was first used to generate a vectorized description of Γ based on Bezier curves, from which the corresponding Ω_Γ subdomain could be easily obtained by imposing the desired stroke thickness. By convention, Ω_Γ was coloured in black, and the remaining pristine region was left in white. This binary vectorized graphic was then exported to a Black and White (B/W) rasterized image with sufficient pixel density, so that it could be read into the FEniCSx-based Python code by the OpenCV v4.10.0 (2024) library. From the ensuing array of integers corresponding to the raster map, the Finite Element nodes falling within Ω_Γ were easily identified on the logical basis that the associated pixel had a stored value of 0.

Another use here given to this digital-optical technique was to define the spatial distribution of characteristic element sizes h, as illustrated in Fig. 9. As previously stated, only the surroundings of Ω_Γ require very fine meshes in order to accommodate the smeared cracks, while the bulk of the fragments can be meshed coarsely for the sake of computational efficiency. Therefore, the region where mesh refinements are required can be easily obtained from the already available vectorized representation of Γ by setting a suitable stroke thickness, naturally larger than Ω_Γ's. By coherence with the procedure in Fig. 8, the black and white regions correspond to the cracked and pristine regions and, by extension, to the smallest h_{min} and

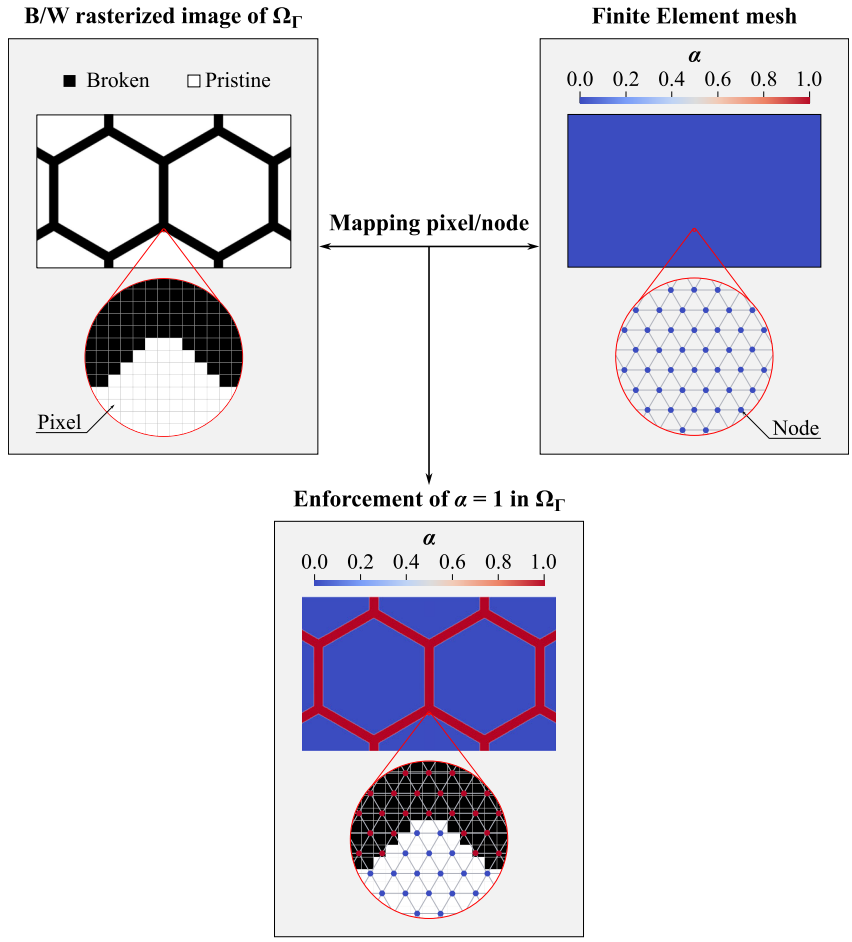


Fig. 8 Schematic description of the technique used for the digital-optical encoding of the Ω_Γ topology

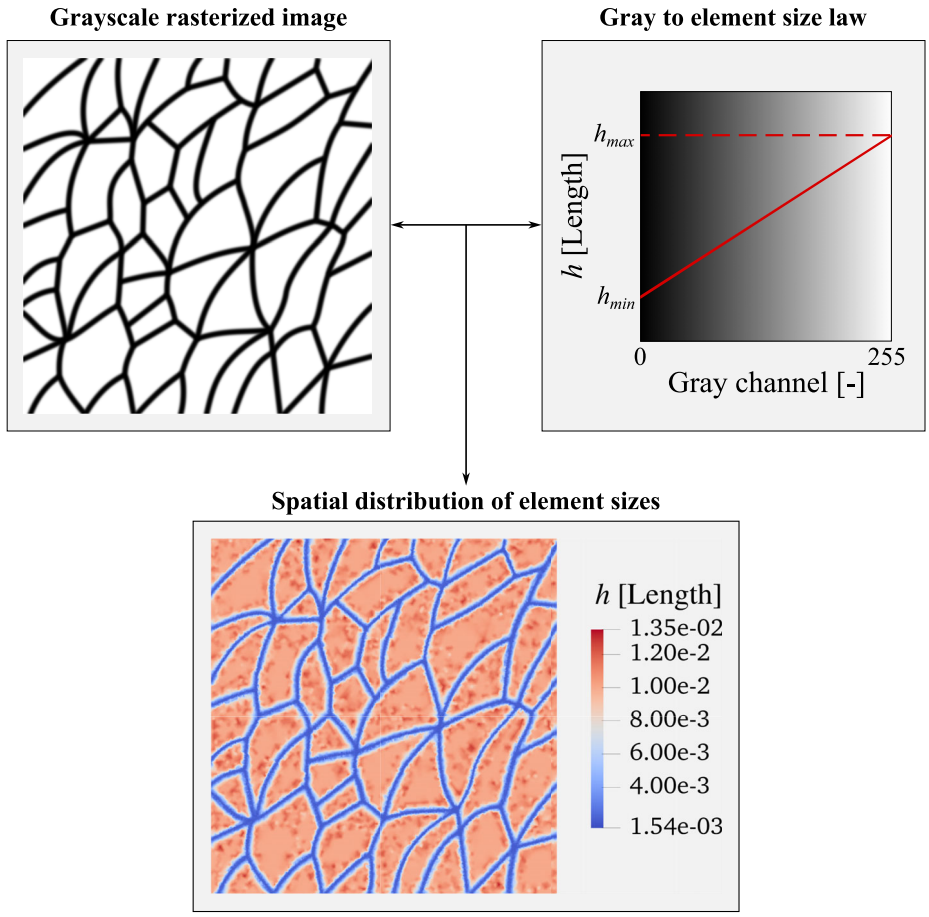


Fig. 9 Schematic description of the technique used for the digital-optical encoding of the spatial distribution of element sizes within Ω. Please note that the conventional 8-bit encoding per channel and pixel is here used

largest h_{max} element sizes (see Fig. 9). Of course, in the proposed PFM-based approach h_{min} corresponds to h_Γ. So as to provide a numerically-convenient continuous definition of the element sizes in space, the black-to-white transition was smoothed into a grayscale by using the blurring effect. This was accompanied by the definition of an interpolation function between the shades of grey and element sizes, for which a simple linear relation was here used. Finally, this information was passed on to the Gmsh mesh generator (Geuzaine and Remacle 2009) through the `meshSizeCallback` function, which takes a position in space and returns the corresponding local values of h.

The herein described digital-optical technique has therefore proven to be highly capable for the definition of complex spatial distributions into numerical models. Furthermore, since it delegates most of the modelling complexity to well-established digital processing pieces of software, the underlying codes for the numerical models can remain mostly unvaried even when being applied to radically different scenarios, hence improving their reliability. Overall, this procedure benefits from the use of rasterized images in two fronts: (i) raster maps are highly efficient data structures memory-wise when it comes to storing spatial distributions of information, and (ii) the ubiquity and popularity of digital images in the latest times has fueled an extensive research and development of techniques for their generation and processing.

References

Alnæs MS, Blechta J, Hake J et al (2015) FEniCS project version 1.5. Arch Numer Softw 3:9-23. https://doi.org/10.11588/ans.2015.100.20553

Ambrosio L, Tortorelli VM (1990) Approximation of functional depending on jumps by elliptic functional via t-convergence. Commun Pure Appl Math 43:999–1036. https://doi.org/10.1002/cpa.3160430805

Amor H, Marigo JJ, Maurini C (2009) Regularized formulation of the variational brittle fracture with unilateral contact: numerical experiments. J Mech Phys Solids 57:1209–1229. https://doi.org/10.1016/j.jmps.2009.04.011

Angelides SC, Talbot JP, Overend M (2022) The influence of fracture pattern on the residual resistance of laminated glass at high strain-rates: an experimental investigation of the post-fracture bending moment capacity based on time-temperature mapping of interlayer yield stress. Glass Struct Eng 7:549–568. https://doi.org/10.1007/s40940-022-00168-y

Baratta IA, Dean JP, Dokken JS et al (2023) DOLFINx: the next generation FEniCS problem solving environment. https://doi.org/10.5281/zenodo.10447666

Bedon C, Fasan M (2024) Post-fracture stiffness and residual capacity assessment of film-retrofitted monolithic glass elements by frequency change. Math Probl Eng 2024:1–16. https://doi.org/10.1155/2024/8922303

Biolzi L, Cattaneo S, Orlando M et al (2018) Post-failure behavior of laminated glass beams using different interlayers. Compos Struct 202:578–589. https://doi.org/10.1016/j.compstruct.2018.03.009

Biolzi L, Casolo S, Orlando M, Tateo V (2019) Modelling the response of a laminated tempered glass for different configurations of damage by a rigid body spring model. Eng Fract Mech 218:106596. https://doi.org/10.1016/j.engfracmech.2019.106596

Bleyer J, Roux-Langlois C, Molinari JF (2017) Dynamic crack propagation with a variational phase-field model: limiting speed, crack branching and velocity-toughening mechanisms. Int J Fract 204:79–100. https://doi.org/10.1007/s10704-016-0163-1

Bourdin B, Francfort GA, Marigo JJ (2000) Numerical experiments in revisited brittle fracture. J Mech Phys Solids 48:797–826. https://doi.org/10.1016/S0022-5096(99)00028-9

Casolo S (1999) Rigid element model for non-linear analysis of masonry facades subjected to out-of-plane loading. Commun Numer Methods Eng 15:457–468

Casolo S (2004) Modelling in-plane micro-structure of masonry walls by rigid elements. Int J Solids Struct 41:3625–3641. https://doi.org/10.1016/j.ijsolstr.2004.02.002

Chambolle A, Conti S, Francfort GA (2018) Approximation of a brittle fracture energy with a constraint of non-interpenetration. Arch Ration Mech Anal 228:867–889. https://doi.org/10.1007/s00205-017-1207-z

Chao Correas A, Reinoso J, Cornetti P, Corrado M (2024) On the (lack of) representativeness of quasi-static variational fracture models for unstable crack propagation. J Mech Phys Solids 186:105573. https://doi.org/10.1016/j.jmps.2024.105573

Corrado M, Chao Correas A, Ventura G (2024) Phase field fracture model for assessing the load bearing capacity of fractured glass. Chall Glas Conf Proc 9:594. https://doi.org/10.47982/cgc.9.594

De Lorenzis L, Maurini C (2022) Nucleation under multi-axial loading in variational phase-field models of brittle fracture. Int J Fract 237:61–81. https://doi.org/10.1007/s10704-021-00555-6

Fei F, Choo J (2019) A phase-field method for modeling cracks with frictional contact. Int J Numer Methods Eng 121:740–762. https://doi.org/10.1002/nme.6242

Francfort GA, Marigo JJ (1998) Revisiting brittle fracture as an energy minimization problem. J Mech Phys Solids 46:1319–1342. https://doi.org/10.1016/S0022-5096(98)00034-9

Geuzaine C, Remacle JF (2009) GMSH: a three-dimensional finite element mesh generator with built-in pre- and post-processing facilities. Int J Numer Methods Eng 79(11):1309–1331. https://doi.org/10.1002/nme.2579

Inkscape Project (2023) Inkscape. https://inkscape.org

Koureas I, Pundir M, Feldfogel S, Kammer DS (2022) On the failure of beam-like topologically interlocked structures. J Mech Phys Solids 259:112029. https://doi.org/10.1016/j.ijsolstr.2022.112029

Kumar A, Bourdin B, Francfort GA, Lopez-Pamies O (2020) Revisiting nucleation in the phase-field approach to brittle fracture. J Mech Phys Solids 142:104027. https://doi.org/10.1016/j.jmps.2020.104027

Lopez-Pamies O, Dolbow JE, Francfort GA, Larsen CJ (2025) Classical variational phase-field models cannot predict fracture nucleation. Comput Methods Appl Mech Eng 433A:117520. https://doi.org/10.1016/j.cma.2024.117520

Lorez F, Pundir M, Kammer DS (2024) Eulerian framework for contact between solids represented as phase fields. Comput Methods Appl Mech Eng 418A:116497. https://doi.org/10.1016/j.cma.2023.116497

Marigo JJ, Maurini C, Pham K (2016) An overview of the modelling of fracture by gradient damage models. Meccanica 51:3107–3128. https://doi.org/10.1007/s11012-016-0538-4

Nielsen JH, Schneider J, Kraus MA (2022) The in-plane expansion of fractured thermally pre-stressed glass panes: an equivalent temperature difference model for engineering glass design. Constr Build Mater 327:126849. https://doi.org/10.1016/j.conbuildmat.2022.126849

OpenCV Project (2024) OpenCV. https://opencv.org

Pham K, Amor H, Marigo JJ, Maurini C (2011) Gradient damage models and their use to approximate brittle fracture. Int J Damage Mech 20:618–652. https://doi.org/10.1177/1056789510386852

Steinke C, Kaliske M (2019) A phase-field crack model based on directional stress decomposition. Comput Mech 63:1019–1046. https://doi.org/10.1007/s00466-018-1635-0

Strobl M, Seelig T (2015) On constitutive assumptions in phase field approaches to brittle fracture. Procedia Struct Integr 2:3705–3712. https://doi.org/10.1016/j.prostr.2016.06.460

Veer FA, Louter PC, Bos FP et al (2008) The strength of architectural glass. Chall Glas Conf Proc 1:419–428. https://doi.org/10.7480/cgc.1

Vicentini F, Zolesi C, Carrara P et al (2024) On the energy decomposition in variational phase-field models for brittle fracture under multi-axial stress states. Int J Fract 247:291–317. https://doi.org/10.1007/s10704-024-00763-w

Williams A, Siegmund T (2021) Mechanics of topologically interlocked material systems under point load: Archimedean and Laves tiling. Int J Mech Sci 190:106016. https://doi.org/10.1016/j.ijmecsci.2020.106016

Yin Z, Hannard F, Barthelat F (2019) Impact-resistant nacre-like transparent materials. Science 364:1260–1263. https://doi.org/10.1126/science.aaw8988

Publisher's Note Springer Nature remains neutral with regard to jurisdictional claims in published maps and institutional affiliations.